Knockout of the muscle-specific E3 ligase MuRF1 affects liver lipid metabolism upon dexamethasone treatment in mice

Laurent Mosoni, Arno Germond, Cécile Coudy-Gandilhon, Mélodie Malige, Agnès Claustre, Coralie Delabrise, Mehdi Djelloul-Mazouz, Yoann Delorme, Julien Hermet, Pierre Fafournoux, et al.

Knockout of the muscle-specific E3 ligase MuRF1 affects liver lipid metabolism upon dexamethasone treatment in mice

Laurent Mosoni[1*], Arno Germond[2], Cécile Coudy-Gandilhon[1], Mélodie Malige[1], Agnès Claustre[1], Coralie Delabrise[1], Mehdi Djelloul-Mazouz[1], Yoann Delorme[1], Julien Hermet[1], Pierre Fafournoux[1], Lydie Combaret[1], Cécile Polge[1], Anne-Catherine Maurin[1] and Daniel Taillandier[1*]

1 Université Clermont Auvergne, INRAE, UNH, Unité de Nutrition Humaine, F-63000 Clermont-Ferrand, France

2 UR370, QuaPA, Qualité des Produits Animaux, INRAE, F-63000 Clermont-Ferrand, France

* Correspondence: laurent.mosoni@inrae.fr; daniel.taillandier@inrae.fr

Short title: MuRF1 influences liver lipid metabolism

Abstract:

In order to preserve muscle mass during catabolic states, investigators are actively searching for a specific inhibitor of MuRF1, the only known E3 ligase able to target muscle contractile proteins for their degradation. However, it is unknown what would be the consequences of such inhibitors on other organs, both in the short and long term. Indeed, skeletal muscles can provide amino acids for liver gluconeogenesis, which is a crucial adaptation for maintaining glucose homeostasis upon elevated energy demands (*e.g.* during prolonged starvation). Comparing 3-month-old wild-type and MuRF1-KO mice, we measured tissue weights, liver glycogen, lipid and protein content, and liver biochemical composition using Fourier Transform Infrared (FTIR) spectrometry in control animals and in dexamethasone (Dex) treated animals. Dex induces a catabolic situation with muscle atrophy and lipid deposits in the liver. In response to Dex treatment, liver glycogen, lipid and protein content increased in wild type (WT) and MuRF1-KO mice. We found that MuRF1 deletion differentially affected organs weights, the liver of KO mice being hypertrophied upon Dex treatment when compared to WT mice. Upon Dex treatment, muscle mass was preserved in MuRF1-KO mice and, by contrast, liver lipid content increased more in these animals than in WT mice. PLS-DA analysis of FTIR showed that the levels of 13 markers were significantly altered in KO vs. WT mice, witnessing profound alterations of lipid, protein and glycogen content in the liver due to the absence of MuRF1. Using Nile red and oil red O lipid staining, we also found that both membrane-linked lipids and intracellular lipid droplets were altered due to the absence of MuRF1. Altogether, it seems that when the liver is deprived of the possibility to obtain amino acids from muscle upon Dex treatment, there is a concomitant increase in tissue weight and anabolic activity.

Introduction

The main function of skeletal muscle is to provide power and strength for locomotion and posture. However, skeletal muscles being the main reservoir of amino acids (AAs) in the body, muscle proteins can be degraded in case of emergency to furnish AAs to the other organs (mainly viscera) [1]. Increased muscle protein breakdown during diseases is an adaptive mechanism that allows the organism to maintain vital functions and that is generally harmless during short-term/acute diseases [2]. Indeed, metabolic alterations of the gut and liver are often present in acute and chronic disease situations, which are often associated with an increased inflammation [3]. As a consequence, the needs of AAs are increased to support a higher energy expenditure, hepatic gluconeogenesis, and the production of acute phase proteins. For example, skeletal muscle is the main production site of alanine in the body during high demand of the organism, which can be achieved through the alanine-glucose cycle [1, 4].

However, during chronic diseases, an uncontrolled and sustained muscle wasting impairs movement, decreases autonomy, but has also detrimental metabolic consequences. Indeed, catabolic states are associated with metabolic alterations of other organs leading to broader deteriorations (food intake disorders, insulin resistance…). In the whole, these disorders lead to patient frailty and impair treatments. For example, muscle atrophy is highly deleterious for cancer patients with cachexia as it alters both the quality of life and the efficiency of treatments, and survival of cancer patients exhibiting muscle wasting is dramatically reduced [5]. Thus, developing strategies to prevent or limit muscle protein loss will contribute to improve patient's health, to maintain life quality and autonomy, and to reduce healthcare costs.

The decrease in muscle mass during diseases is attributable to an alteration of proteostasis mainly due to an increased protein degradation, which affects the size of muscle fibers rather than decreasing their number [6, 7]. Proteolysis activation for rapid degradation of sarcomeric proteins is thus the main cause of muscle atrophy, the ubiquitin proteasome system (UPS) and autophagy being the main proteolytic systems involved [6, 8].

The UPS is crucial as it controls the degradation of the bulk of cellular proteins and also represses protein synthesis [6]. The UPS targets the proteins to be degraded by linking covalently a ubiquitin (Ub) chain to the substrates thanks to an enzymatic cascade (E1, E2, E3), which enables the recognition and the degradation of the targets by the 26S proteasome. The

muscle ring finger-1 (MuRF1) E3 ligase is muscle-specific and possesses a crucial role during the muscle atrophy process as MuRF1 is so far the only known E3 ligase able to target the contractile proteins for their degradation [9, 10, 11]. Inhibiting MuRF1 is thus a potential strategy for sparing muscle mass in patients suffering from chronic diseases. Accordingly, MuRF1 KO in mice is known to protect muscle mass in several catabolic situations like hindlimb suspension [9], glucocorticoid treatment [9, 12] or cancer [13]. Thus, targeting MuRF1 by using chemical inhibitors is a strategy that started to be developed with some positive results. Using MyoMed-205, the only MuRF1 inhibitor so far usable *in vivo*, a partial protection of the diaphragm muscle was observed either in mice encountering myocardial dysfunction or after diaphragm denervation [14, 15].

While strong inhibitors of MuRF1 are still not available, one can hypothesize that maintaining muscle protein mass by using pharmaceutical approaches in chronic disease patients may have a negative impact on other organs. Indeed, MuRF1 inhibition could impede the liver from obtaining a sufficient amount of AAs during acute catabolic states, thus impairing the production of inflammatory proteins and neoglucogenesis. In the long term, MuRF1 inhibition could also alter daily exchanges between muscle, intestine, and liver, which may impact the overall metabolism of the latter organs [16]. To the best of our knowledge, this aspect has not been studied in the literature. To address this hypothesis, MuRF1-KO mice provide an opportunity to test the impact of muscle sparing on other organs during catabolic situations. Indeed, the absence of MuRF1 in KO animals mimics total inhibition of this E3 ligase. Glucocorticoid treatment (e.g. Dexamethasone, Dex) is known to drastically increase both gluconeogenesis [17, 18, 19] and protein synthesis [20, 21] in the liver, while it induces muscle atrophy through increased UPS-dependent degradation, notably by increasing MuRF1 expression [9, 12]. In addition, despite being only expressed in muscles, an overexpression of MuRF1 is also known to modulate both glucose and glycogen metabolism in the liver [22], further suggesting that altering MuRF1 levels for preserving muscle mass should take into account potential side effects on other organs.

In this work, due to the crucial dialog between the liver and skeletal muscles [23], we addressed whether muscle sparing in Dex-treated MuRF1-KO mice impact liver metabolism. We found that lipids dramatically accumulated in the liver of MuRF1-KO mice. In particular, using Fourier Transform Infrared (FTIR) spectrometry, we showed that the response of lipid metabolism to Dex treatment was significantly different in MuRF1-KO mice compared to wild-

type mice. We also found significant differences between control wild-type and control MuRF1-KO mice suggesting long-term adaptations to MuRF1 deletion.

Materials and method

Animals and Tissue Collection:

The experiments were conducted following the guidelines set forth by the French National Research Council Guide for the Care and Use of Laboratory Animals. The study received national authorization to perform animal experiments under project number 2017042115497506 (authorization #9204). All animal procedures were performed in accordance with ethical guidelines and to minimize pain and distress.

Three months old male C57BL/6 mice were used for the experiments. Two strains of mice were included in the study: wild type (n = 12) and MuRF1-KO mice (n = 12). MuRF1-KO mice were a gift from Pr. S. Labeit (Medical Faculty Mannheim, University of Heidelberg) and Pr. V. Adams (Heart Center Dresden). Throughout the experiment, the animals were housed in a temperature-controlled environment (22 ± 1 °C) with a 12:12 h light-dark cycle. Food was available only from 8:00 AM to 5:00 PM. The mice were acclimated to these conditions for 1 week before the onset of the study.

Water-soluble dexamethasone (Dex, Sigma) was administered to 6 mice of each strain through drinking water, the groups being labeled: WT, WT-Dex, KO and KO-Dex. The treated group received a daily dose of 5 mg/kg of Dex for 5 days. Preliminary experiments did not find any difference in food consumption within Dex treatment (data not shown) but food offered and leftovers were weighed and taken into account for calculating daily food intake. The last day of experiment, all animals were given access to food only from 8:00 AM to 9 AM. Subsequently, access to food was removed, and mice were euthanized by cervical dislocation after 5-8 h, *i.e.* in the post absorptive state.

The gastrocnemius muscles of both hind legs were excised, weighed, and rapidly frozen in liquid nitrogen.

The liver was excised, rinsed, dried, and weighed. Three-fourths of the liver tissue was frozen in liquid nitrogen, while one lobe (around one-fourth of total liver) was frozen in cooled isopentane for histochemistry analyses. The intestine was excised, emptied, cleaned, dried, and weighed. The jejunum and colon were then frozen in liquid nitrogen. Other organs

(heart, kidneys, and spleen) were excised and weighed. All collected tissues were promptly stored at −80 °C until further analysis.

Biochemical analyses

Liver tissue was crushed in liquid nitrogen, and aliquots were used to determine protein and glycogen content. Protein content was measured using the Biorad (Hercules, CA, USA) protein assay following extraction in Tris-based buffer (40 mM Tris, pH 7.4; 5 mM EGTA, 1 mM EDTA; 0.5 % Triton X-100; 1 mM PMSF, 10 µg/ml leupeptin). Glycogen content was measured according to the method described by Keppler and Decker [24]. Briefly, glycogen was hydrolyzed by an amyloglucosidase and the glucose content was specifically determined through the sequential action of an hexokinase a glucose 6-P dehydrogenase. The resulting NADPH was measured at 340 nm.

Liver histochemistry

Liver cross-sections (10 µm thick) were obtained using a cryostat (Microm, Francheville, France) at -25°C. Neutral lipids present in lipid droplets were visualized using oil red O [25]. Briefly, oil red O (ORO, Sigma) stock solution (500 mg/ml ORO in 60% triethylphosphate in water (v/v)) was diluted with 0.67 vol water and filtered before use. Cross-sections were air-dried, incubated in 100 % acetone for 1 hour, washed thrice with PBS, and were then incubated with ORO diluted solution for 20 min, and washed thrice with water. The slides were mounted with a water-soluble mounting medium (IMSOL Mount VWRK4058). Image acquisitions were captured with a high-resolution ORCA-Flash4.0 LT+ Digital CMOS camera coupled to a IX-73 microscope (Olympus) and Cell-Sens dimension software (Olympus Soft Imaging Solutions, Münster, Germany). Images were analyzed with ImageJ2 v. 2.14.0/1.54f (http://rsb.info.nih.gov/ij) to determine the area of lipid droplets (LD).

Nile Red staining of lipid membranes was performed as follows. NILE red (7385-67-3, Sigma) stock solution (3 mg/ml ORO in ethanol) was diluted with 75% glycerol and 25% distilled water. Liver cross-sections were incubated in this solution during 30 minutes in the dark, washed thrice with PBS and once with water. The slides were mounted with a water-soluble mounting medium (IMSOL Mount VWRK4058) and coverslips.

Glycogen deposits were visualized using Periodic Acid Schiff (PAS) staining. The slides were immersed in PAS solution for 5 minutes and washed thrice with distilled water. The slides were immersed in Schiff's Reagent for 15 minutes and washed thrice in tap water for 5

minutes. The slides were dehydrated, cleared and sections were mounted in EUKITT mounting medium (15320 Electron microscopy sciences) and analyzed as described above for lipids.

Fourier-transform infrared (FTIR) measurements and pre-processing

Liver cross-sections (10 µm thick) were obtained using a cryostat (Microm, Francheville, France) at -25°C and placed onto BaF_2 slides, then analyzed with an FTIR microscope (Thermo Scientific iN10, Thermo Fisher Scientific, Madison, WI, USA) equipped with a liquid nitrogen-cooled detector.

After the acquisition of a mosaic image of the sample, random areas were chosen to acquire 30 spectra calculated from the average of 256 exposures using a 30 µm aperture. The background signal from the BaF2 plates was obtained with 256 exposures near the tissue sample. Spectra were acquired at a resolution of 2 cm^{-1} in the range 670–2000 cm^{-1}. A total of 7858 spectra were recorded. Background signal from BaF2 was subtracted. Spectra were then further processed. We applied a baseline correction using a polynomial fitting (5^{th}-order, 200 iterations; [26]) followed by a vector normalization. The area from 800 to 1780 cm^{-1} corresponding to the fingerprint area was considered for subsequent statistical and machine-learning analyses.

Statistical analyses and machine learning:

A t-SNE model (5 PCs) was computed to visualize the heterogeneity of the spectral measurements along the four treatments (WT, WT-Dex, KO, KO-Dex, n = 7,858). Using the same data, a Support Vector Machine (SVM) model was computed to test the ability to identify each treatment based on the spectral measurements. The radial basis function (RBF) kernel was considered. The training dataset was selected by randomly taking 70% of the spectral dataset. The model was tested using the remaining 30%. This process was iterated 100 times, and the model outputs were averaged. The output of the SVM classification is a confusion matrix showing the percentages of predicted spectra that are rightly classified when compared to true spectra. These models were computed using Orange data mining software version 3.33 [27].

To identify, in an objective manner, the spectral frequencies that are most associated to each treatment group (hereafter called biomarkers), we utilized the Projection on Latent Variables (PLS-DA). To compare treatments, we computed models 2 by 2 to test for the treatment effects. Specifically, we first tested the effect of MuRF1-KO on non-treated mice (WT vs. KO). Then, we tested the effect of Dex on WT mice (WT-CT vs. WT Dex) and the effects of the Dexamethasone in the KO group, using the comparison KO-CT vs KO-Dex. Last, we compared the groups KO-Dex and WT-Dex, to understand the effects of MuRF1-KO upon Dex treatment. After the model classification, we extracted the Variable Importance in Projection (VIP scores), which reflect the biomarkers important for treatment comparisons.

We performed two-way variance analyses (ANOVA) on tissue weight, and liver lipid, protein and glycogen content, and on the FTIR-identified biomarkers to test the effect of strain (WT vs MurF1-KO), the effect of treatment (Control vs. Dex), and the interaction between these 2 factors. In addition, we analyzed the effects of time, treatment and strain on food intake and weight by repeated time variance analysis. ImageJ2 data from Nile Red lipid staining were log10-transformed and analyzed using one-way ANOVA.

Results

Evolution of food intake and body weight before and during Dex treatment

Dex treatment may interfere with food consumption and some studies found an increased food intake in Dex-treated mice [28], in contrast with depressed food intake in rats [20, 29]. In our study, repeated time variance analysis showed that there was no effect of Dexamethasone treatment on food intake (Figure 1A). However, in WT animals, food intake tended to decrease in response to Dex treatment, (Figure 1A), and food consumption tended to be slightly lower in WT mice compared to KO animals (significant only at days 3 and 5). However, this may only partially explain the overall body weight modifications (see below). Repeated time variance analyses showed that the effect of Dex on body weight (Figure 1B) was significantly different in WT mice and MuRF1-KO mice. WT animals exhibited a stable weight, and reduced their body weight in response to Dex treatment in accordance with the catabolic effect of high doses of glucorticoids [30]. By contrast, MuRF1-KO animals progressively gained weight with no effect of Dex treatment. As a result, body weight was significantly higher in MuRF1-KO mice than in WT mice during Dex treatment (+16%, $p <$

0.05) in accordance with previous studies that detected an increased weight of different muscles when MuRF1 is absent [31].

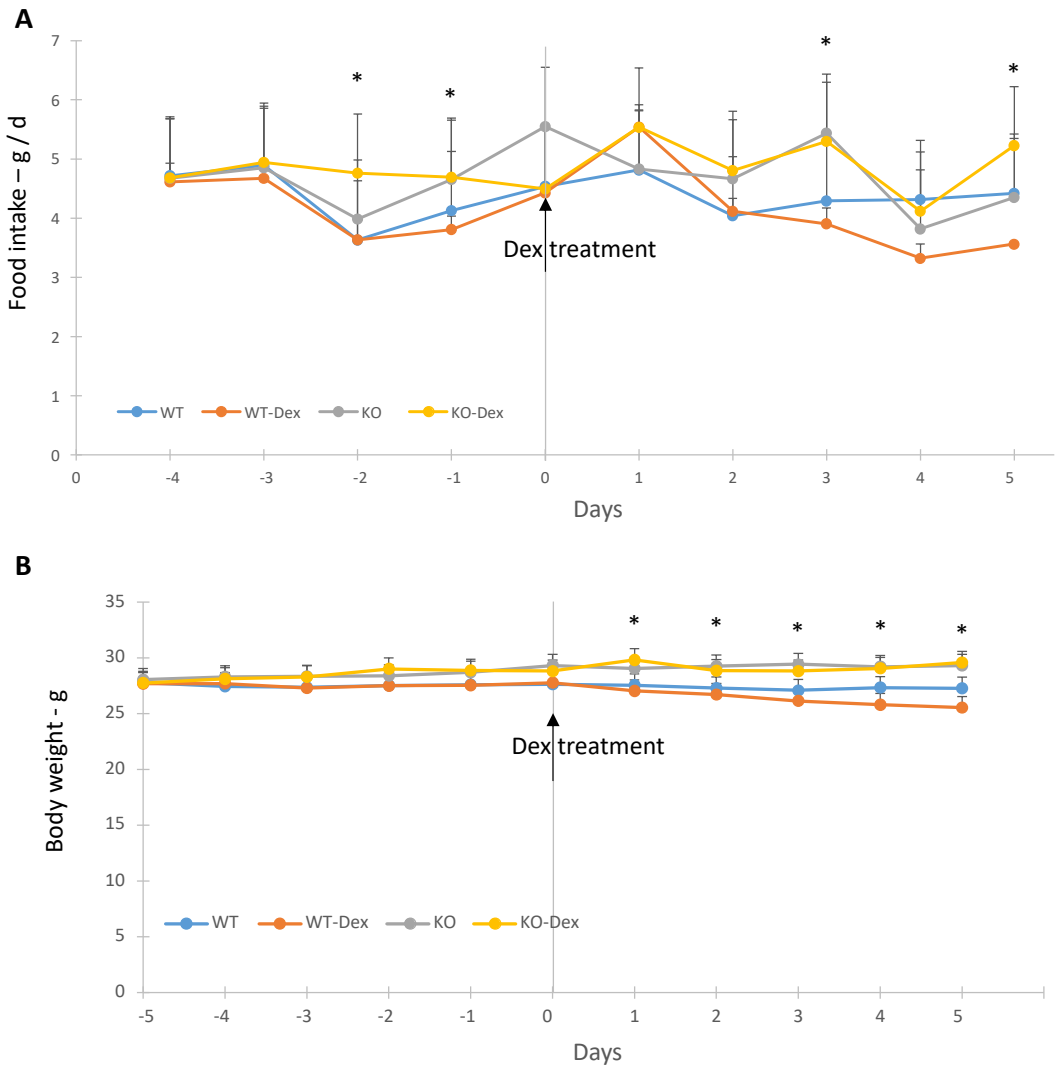

Figure 1: A) Evolution of food intake (A) and body weight (B) before and during Dex treatment in wild type and MuRF1-KO mice

Wild type and MuRF1-KO mice were treated or not with Dexamethasone (daily dose of 5 mg/kg in drinking water) for 5 days. Food intake and body weights were recorded daily before and during the treatment. Means ± SEM are given; n = 6 per group. Repeated time variance analysis was performed *: mean value for KO and/or KO-Dex significantly higher than for WT and WT-Dex groups, $p < 0.05$.

Dex: dexamethasone; WT: wild type mice; WT-Dex: wild type Dex-treated mice; KO: MuRF1-KO mice; KO-Dex: MuRF1-KO Dex-treated mice.

Impact of Dex treatment on organs' weight.

As expected, the gastrocnemius weight significantly decreased upon Dex treatment in WT animals while muscle mass was partially spared in MuRF1-KO animals (P=0.07) (Figure 2A). We found an increased heart weight (+13-15 %, $p < 0.05$) in MuRF1-KO mice with no effect

of Dex treatment (Figure 2B), which is in accordance with the presence of MuRF1 in any muscle type (skeletal, smooth and cardiac). Heart hypertrophy in MuRF1-KO animals is in accordance with the literature [32].

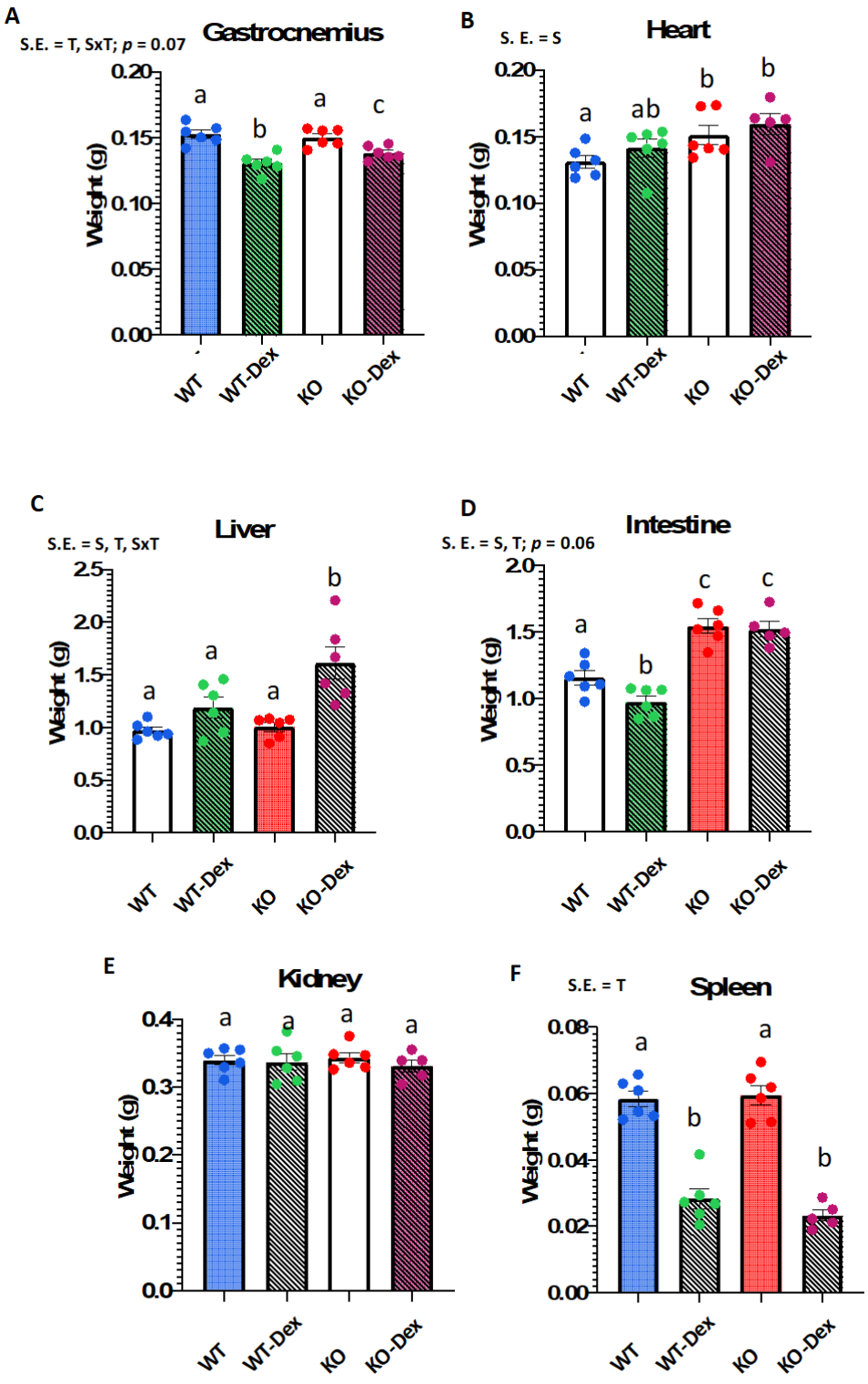

Figure 2: Effect of Dex treatment on tissue weights in WT and MuRF1-KO mice

WT and MuRF1-KO mice were treated or not with Dexamethasone (daily dose of 5 mg/kg in drinking water) for 5 days. Significant effects (S.E.) of variance analysis are reported: T = Dex treatment; S = strain; SxT = interaction between Dex treatment and strain. Means ± SEM are given; n = 6 per group. Mean values affected by different letters are significantly different ($p < 0.05$).

We then addressed the effect of the genotype on other organs following Dex treatment as we expected some alterations due to the protection of the skeletal muscles. Liver weight was significantly higher in MuRF1 KO mice when compared to WT mice (Figure 2C). Dex treatment also increased liver weight in WT animals, and this hypertrophy was even exacerbated in MuRF1-KO animals (Figure 2C).

As in the heart (but at a higher degree), small intestine weight was significantly higher in MuRF1-KO than in WT mice (+34-56%, $p < 0.05$, Figure 2D). By contrast with the liver, Dex treatment decreased small intestine weight in WT mice with no effect in KO animals (Figure 2D).

While kidney weight was unaffected by the genotype and Dex treatment (Fig 2E), spleen weight was dramatically decreased in Dex-treated animals with no effect of MuRF1 deletion (Figure 2F). Such a decrease in spleen weight constitutes a marker of the effectiveness of Dex treatment [33, 34].

FTIR vibrational spectroscopy showed that the muscle-specific MuRF1 E3 ligase affects carbohydrate, lipid and protein content of the liver

To address in the liver the impacts of Dex treatment and muscle-specific MuRF1 deletion, we analyzed liver extracts with FTIR vibrational spectroscopy coupled with machine learning approaches (Figure 3, Tables 1 and 2). FTIR provides important information regarding the macromolecular contents (DNA, protein, lipids, etc.) in a cell or tissue sample through the analysis of spectra specific of biochemical linkages (e.g. the COH of glucose) [35]. FTIR is also able to differentiate between diseased and non-diseased states, and treatments. Spectral data unequivocally distinguished strong differences in the fingerprint area depending on the treatment and the genotype (Figure 3A), and we found that Dex treatment greatly modified the abundance of all the chemical species detected by FTIR (proteins, lipids, carbohydrates, etc.). The averaged spectra of each group of mice are represented for visualization purposes

(total n = 7858). The graphic clearly shows the effect of Dex treatment on liver cells. Notably, the intensity of peaks in the spectral range from 900 to 1200 cm^{-1} (associated with carbohydrates, glucose, aromatic compounds, and lipids) was strongly increased in in Dex-treated mice, whatever the genotype (Figure 3A). Likewise, the intensity of the peak at 1750 cm^{-1} (associated with triglycerides) was significantly higher for Dex-treated mice. The peaks at 1540 and 1652 cm^{-1}, respectively associated with saturated lipids and C-C bond (Amide I, protein) (Table 2) were lower in the WT-Dex and KO-Dex treatments.

A

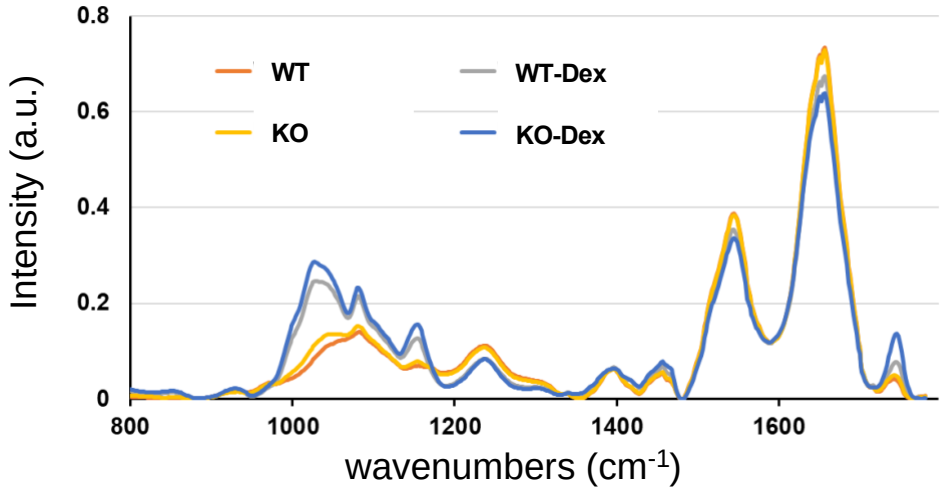

B

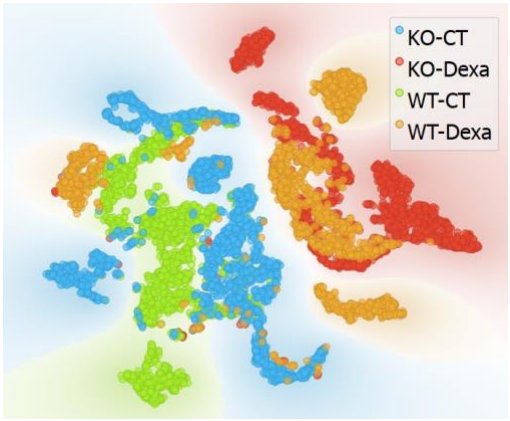

C

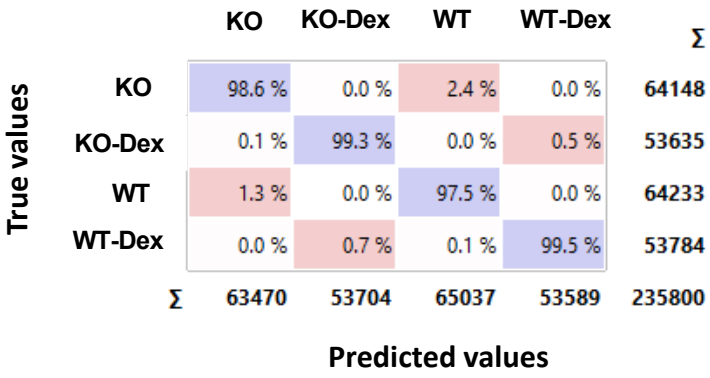

Figure 3: FTIR analysis of the effects of Dex treatment on liver biochemical composition in WT and MuRF1-KO mice. A) Average of normalized spectral intensities for each treatment B) t-SNE plot of 7858 spectra obtained on liver tissue preparation of mice (n = 4-5 per group) subjected to the different treatments (KO-Dex, KO, WT- Dex, WT). The plot indicates strong heterogeneity between mice. However, the KO- Dex group appears more homogeneous as samples of mice liver from this group could not be distinguished. C) Confusion matrix of the SVM model. The confusion matrix shows the results from five iterations of SVM models

(training data 70% / test data 30%). Results indicate that the spectral signatures of mice liver cells enable to predict the 4 treatments accurately.

Table 1. Classification of spectra of lever cells using PLS-DA models (on test datasets) that consider pairs of treatments.

Tested group	Biological Effect	Model complexity (LVs number)	R^2 pred.	Prediction score (sensitivity & specificity for test data)
WT vs. KO	Effect of KO	4	0.413	Sensitivity: 0.87 / 0.733 Specificity: 0.733 / 0.87
KO vs. KO-Dex	Effect of Dex treatment in KO mice	3	0.773	Sensitivity: 0.984 / 0.998 Specificity: 0.998 / 0.984
WT vs. WT-Dex	Effects of Dex treatment in WT	3	0.764	Sensitivity: 0.995 / 0.951 Specificity: 0.951 / 0.995
WT-Dex vs. KO	Crossed Response of KO and Dex	3	0.725	Sensitivity: 0.792 / 0.937 Specificity: 0.937 / 0.792
WT-Dex vs. KO-Dex	Effect of KO upon Dex treatment	6	0.62447	Sensitivity : 0.944 / 0.936 Specificity : 0.936 / 0.944

To visualize the heterogeneity of mice liver composition, a t-distributed stochastic neighbor embedding (tSNE) model was computed based on the spectral signatures (total n = 7858) of liver cells. Figure 3B shows that the spectral composition of mice livers forms distinct groups for each individual (Figure 3B). In this two-dimensional space, we did not observe any treatment effect, except the KO-Dex group, for which spectral of the 6 mice (n = 6) are clustered together.

Interestingly, despite the heterogeneous liver composition of mice, non-linear models such as Support Vector Machine (SVM), and linear regression models (PLS-DA) classified the treatments based on spectral signatures of liver cells with high accuracies (Figure 3C, Table 1). Figure 3C displays the results of SVM models trained on 70% of the data and tested on the remaining 30% over a hundred iterations. The SVM models classified all spectra with

high accuracies ranging from 97.5 to 99.5 %. These results suggest that the spectral data contain features that are highly specific to either Dex treatment or the genotype. Important wavelengths responsible for the SVM classification were extracted. We wanted to test notably the effects of MuRF1 deletion or the Dex treatment. To do so, we then performed comparisons of pairs of treatments using PLS-DA (Table 1). Again, the linear models performed well in terms of sensitivity and specificity, which indicates that significant statistical variations occur when comparing pairs of treatments. These analyses provide a strong basis to support that biomarkers specific to each treatment can be objectively extracted from spectral measurements. To do so, the VIP scores of the PLS-DA models were extracted to identify the wavelengths of importance within the biological comparisons (Figure 4 and S1). Spectral peaks with VIP scores above a threshold of 1 were considered of interest and considered as biomarkers/discriminating biochemical characteristics in Table 2. When comparing KO and KO-Dex mice, we found biomarkers associated with aromatic compounds, such as Phe and Tyr, which are important components of proteins and carbohydrates (~1002 cm^{-1}), as well as multiples markers of carbohydrates content and notably glucose (~1028, ~1084 cm^{-1}, ~1155 cm^{-1}). We also found markers of saturated lipids (~1465 cm^{-1}), and nucleic acids (1079 cm^{-1}) (Figure S1, Table 2). These results indicate that Dex treatment increased the glucose storage and the lipid content of liver cells in KO mice. To support the above results, we performed a two-way variance analysis on the intensity of the peaks identified from VIP scores (Table 2). For all the identified biomarkers, there was a marked effect of Dex treatment. For the peaks associated with carbohydrates (~ 933, ~993, ~1002, ~1028, ~1066, ~1079, ~1084, ~1153 cm^{-1}), the intensities increased in response to Dex treatment. For peaks ~1540, ~1560, ~1646, ~1652, and ~1658 cm^{-1}, which are associated with proteins, the intensities decreased thus indicating liver protein loss in Dex-treated animals. The increase of ~1465 and ~1745 cm^{-1} peaks were also significant, suggesting the molecular composition of lipids was modified upon Dex treatment.

Table 2. Wavelengths of interest identified by VIP scores, and their associations with molecular composition. Results of two-way ANOVA analysis are also shown.

	Associated chemical bounds & molecules	P associated with 2-way variance analysis

Wavenumbers selected by VIP > 1		Strain effect	Treatment effect	Interaction effect
~933 cm^{-1}	–O–C linkage, C–C stretch., α-helix, proteins	0.33	0.0032	0.16
~993 cm^{-1}	–COH from glucose	0.26	0.0002	0.69
~1002 cm^{-1}	–CO group, aromatic compounds, Phe, Tyr.	0.28	0.0002	0.78
~1028 cm^{-1}	$–CH_2OH$ groups associated with carbohydrates, and glucose.	0.29	0.0002	0.91
~1066 cm^{-1}	–CO stretching ribose.	0.34	0.0003	0.99
~1079 cm^{-1}	$–PO_2^-$ groups associated with RNA and DNA.	0.30	0.0002	0.95
~1084 cm^{-1}	$–PO_2^-$ groups, associated with DNA	0.30	0.0002	0.95
~1155 cm^{-1}	–COH groups & absorption peak for C-O-C, such as in glucose	0.07	0.0001	0.39
~1465 cm^{-1}	$–CH_2$ groups associated with saturated lipids, phospholipids.	0.0035	0.0001	0.0534
~1540 cm^{-1}	β-sheets associated to Amide II, saturated lipids	0.26	0.0027	0.58
~1560 cm^{-1}	Ring base, possibly related to Amide II	0.13	0.0076	0.50
~1646 cm^{-1}	Amide I of proteins.	0.20	0.0001	0.38
~1650-1652 cm^{-1}	C=O associated with Amide I of proteins, α-helix of proteins.	0.21	0.0003	0.40
~1658-1660 cm^{-1}	υ(C⍵C) cis, NH_2 associated with guanine, Amide I, uracyl.	0.13	0.0001	0.34
~1747 cm^{-1}	C=O of triglycerides, ester groups of cholesterol or phospholipids	0.0042	0.0001	0.03

Variable Importance in Projection (VIP) scores extracted from PLS models enabled identifying objectively the biomarkers associated with each biological effect. Thirteen peaks belonging to various molecules (lipids, carbohydrates, proteins, etc.) were defined as differentially expressed in WT and KO animals. The data were further analyzed using a two-way ANOVA, which showed that lipid

modifications were the chemical species the most impacted by the genotype. Dex treatment was highly impactful on all the chemical species selected from VIP scores.

To address the effect of MuRF1, we considered first the WT and KO mice without Dex treatment (Figure 4). The highest VIP scores highlighted biomarkers associated with proteins, and carbohydrates (~1002 cm^{-1}, ~1028, and ~1155 cm^{-1}), saturated lipids (~1465 cm^{-1}), and nucleic acids (~1079 cm^{-1}). Then, the comparison between WT-Dex and KO-Dex showed markers of proteins secondary structures (~ 1540 cm^{-1}) and of the C–C stretch and α-helix of proteins (~933, ~1066, and ~1646 cm^{-1}), and a ring base (~ 1560 cm^{-1}), which is possibly related to Amide II according to previous work [36] (Figure S1, Table 2). These evolutions strongly suggest an increase in glycogen and lipid content and a decrease of protein content in KO mice, which we ought to verify with further analysis (see below). For peaks at 1465 cm^{-1} and 1745 cm^{-1}, in addition to the significant effect of Dex, variance analysis showed that there was a significant effect of the strain, and a significant interaction between the effects of strain and Dex-treatment, both peaks being associated with phospholipids. For both peaks, the intensity increased in response to Dex, and this increase was more marked in MuRF1-KO mice.

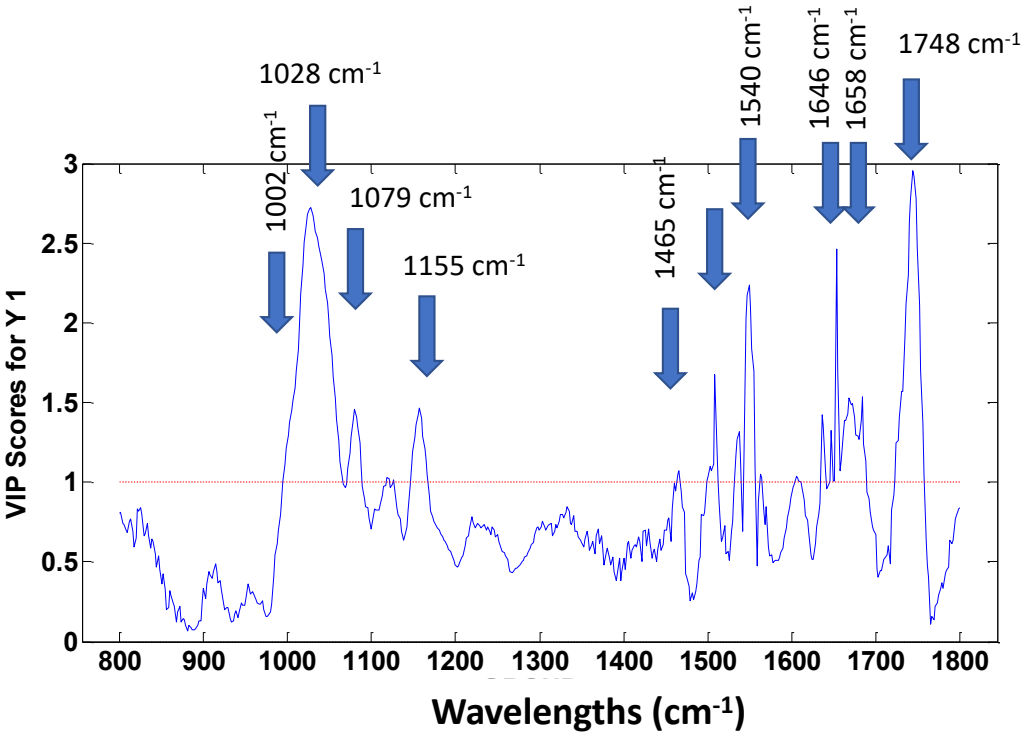

Figure 4: Variable In Projection (VIP) scores extracted from PLS-DA model testing the MuRF1 deletion effect by comparing WT and KO mice. Values above 1 are considered as significant.

The graphic shows 13 biomarkers associated with the KO effect. The highest VIP scores highlighted biomarkers associated with proteins and carbohydrates (~1002 cm^{-1}, ~1028, and ~1155 cm^{-1}), saturated lipids (~1465 cm^{-1}), and nucleic acids (~1079 cm^{-1}). Other comparisons (*e.g.* effect of Dex) are shown in Figure S1.

Quantitative assays of liver protein, glycogen and lipid content

The muscle-specific deletion of MuRF1 in muscles differentially impacted other organs, an effect that was detectable even in absence of any challenge for the small intestine. FTIR was able to detect alteration of liver composition and, combined with the known interorgan relationships between skeletal muscles and the liver, we decided to further investigate the impact of MuRF1-KO in the liver.

We first found that liver hypertrophy was not due to a modification of protein concentration (Figure 5A) but to total protein accretion (Figure 5B), potentially due to hyperplasia as liver cell diameter was similar in WT and KO animals, whatever the treatment (Figures 6 and 7). Liver total protein content was also significantly higher in MuRF1-KO than in WT mice.

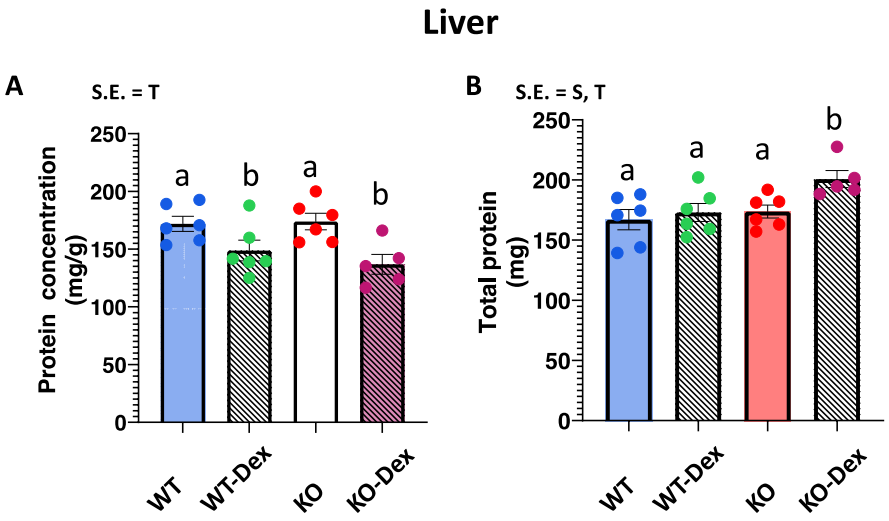

Figure 5: Effect of Dex treatment on liver protein concentration (A) and protein total amount (B) in WT and MuRF1-KO mice

WT and MuRF1-KO mice were treated or not with Dexamethasone (daily dose of 5 mg/kg in drinking water) for 5 days. Protein content was determined as indicated in the methods section. Significant effects (S.E.) of variance analysis are reported: T = Dex treatment; S = strain; SxT = interaction between Dex treatment and strain. Means ± SEM are given; n = 6 per group. Mean values affected by different letters are significantly different ($p < 0.05$).

To confirm the above results, we performed biochemical and/or staining assays to quantify the glycogen and lipid content in liver samples. The liver glycogen content was evaluated using Schiff staining and an enzymatic assay (Figure 6). We found a dramatic increase in glycogen concentration in Dex-treated animals with almost uniform staining of the liver cells (Figure 6 C-D), when compared to non-treated mice (Figure 6A, B). Indeed, based on enzymatic activity, glycogen concentration increased 7.5 and 4-fold in WT and MuRF1-KO mice respectively (Figure 6E). There was also a tendency for higher glycogen content in MuRF1-KO animals when compared to WT mice (Figure 6E-F) but it was more the aspect of glycogen granules that was affected by MuRF1 deletion.

Lipid accumulation was addressed in the liver by either Nile Red or oil red O staining (Figure 7), the former being more specific of membrane-included lipids [38, 39] and the latter revealing intra cytoplasmic lipid droplets (fat storage) [25, 39].

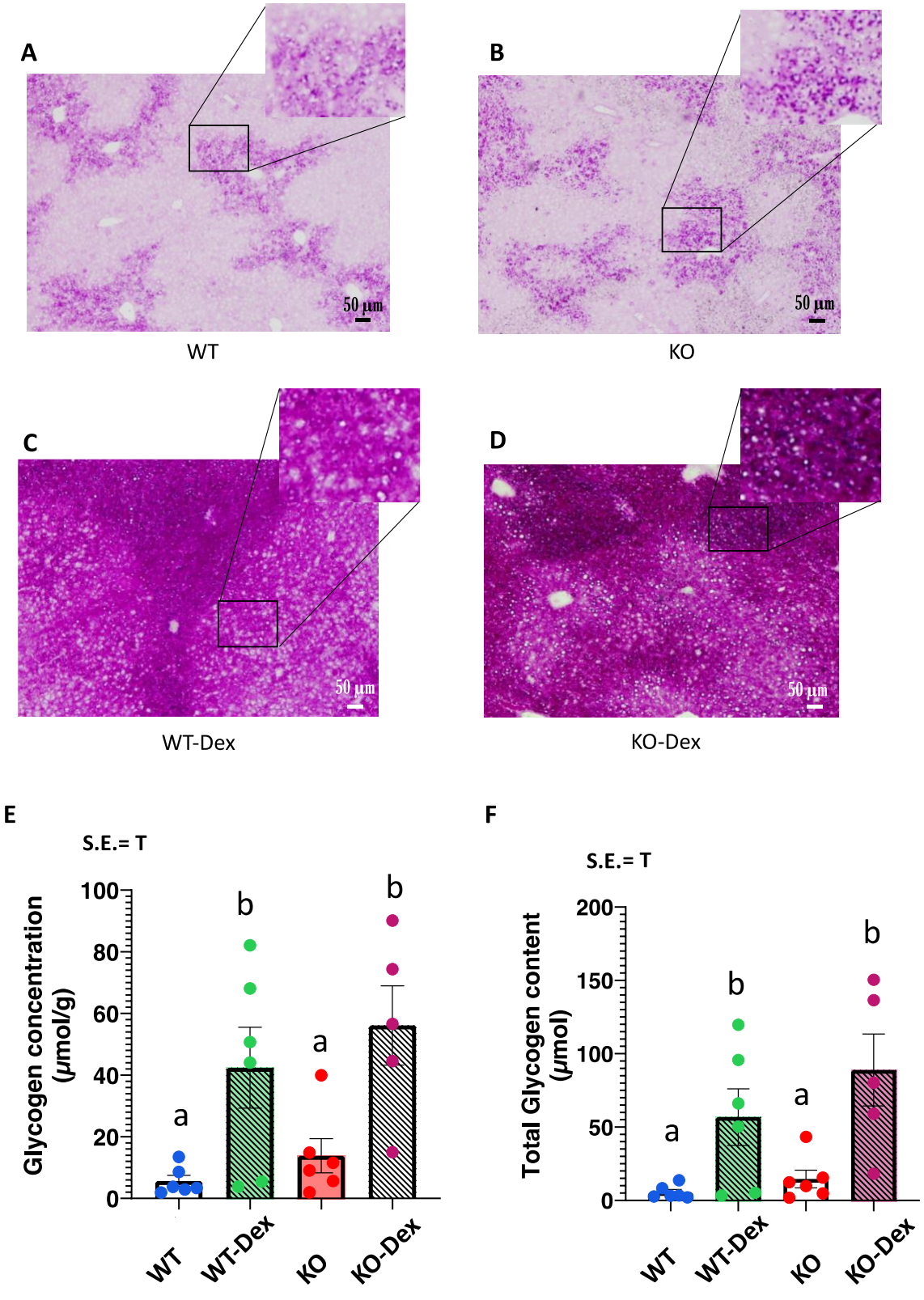

Figure 6: Effect of Dex treatment on liver glycogen content in WT and MuRF1-KO mice. WT and MuRF1-KO mice were treated or not with Dex (daily dose of 5 mg/kg in drinking water) for 5 days. A-E, liver slides were used for addressing glycogen content (see methods section for details) that was visualized by microscopy using PAS staining (see methods section for details). Image acquisitions were captured with a DP23 CMOS camera coupled to

a IX-73 microscope (Olympus). Saturation of the signal in Dex-treated mice did not allow ImageJ (ImageJ2 v. 2.14.0/1.54f) quantification. E, glycogen concentration was determined following hydrolysis by an amyloglucosidase as described by Keppler and Decker [24] and expressed in µmol of glucose per g of liver ; F: Total liver glycogen content expressed in µmol of glucose. Magnification of representative zones was performed using the OMERO software [37].

Dex treatment induced enhanced Nile Red staining in the liver from WT mice (Figure 7A-B), which was further increased in MuRF1-KO animals (Figure 7 C-D). This reflects an increased level of membrane-linked lipids including lipids present in organelles [38] and thus a potential increased area occupied by organelles, including - but not limited to – lysosomes. Globally, there was more vesicle-like particles and they tended to be bigger in WT Dex-treated animals. This effect was largely accentuated in MuRF1-KO animals, particularly for big vesicles (Fig. 7E). Intracellular lipid droplet staining using oil red O indicated that Dex treatment also promoted lipid accumulation in WT animals (Figure 7F, G), which was further increased in MuRF1-KO mice (Figure 7H, I). Altogether, profound macroscopic alterations of the liver appear upon deletion of the muscle-specific MuRF1 E3 ligase, these alterations being exacerbated when the animals are challenged by glucocorticoid treatment.

Discussion

The beneficial effect of MuRF1 inhibition on muscle preservation during catabolic situations is now well established and was confirmed in the present study. MuRF1 is present only in skeletal, cardiac and smooth muscles, thus MuRF1 inhibition should not affect other tissues than muscles. However, tissues interact in the body, in particular during catabolic states, and the inhibition of MuRF1 could have indirect consequences in other tissues than muscle. This aspect was very little studied in the literature. Using MuRF1 KO mice, we showed that there were indeed differences in other tissues between WT and MuRF1-KO mice, either in control or in Dex-treated mice.

The general effects of Dex treatment that we observed in liver through classical biochemical measurements (accumulation of glycogen and lipids) and through the FTIR approach (accumulation of glycogen, lipids, and modification of secondary structure of proteins) were already described [15, 17, 40], indicating that MuRF1-KO animals exhibited a similar (although not identical) behavior to WT animals regarding Dex treatment. While the concentration and

total amounts of glycogen and lipids were increased in liver in response to Dex, total amount of protein was increased but protein concentration was reduced, in accordance with the decrease in the peaks associated with proteins in the FTIR assays. This suggest that the decreased protein concentration was probably related to the increased proportion of glycogen and lipid in liver from MuRF1-KO mice.

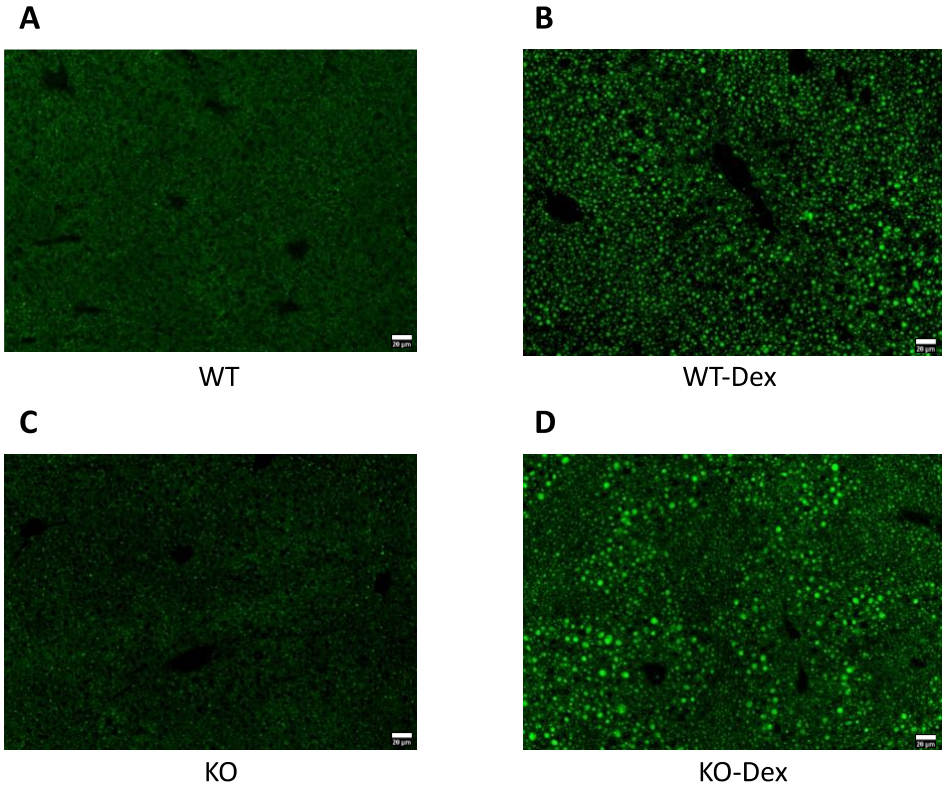
A
B
WT
WT-Dex
C
D
KO
KO-Dex

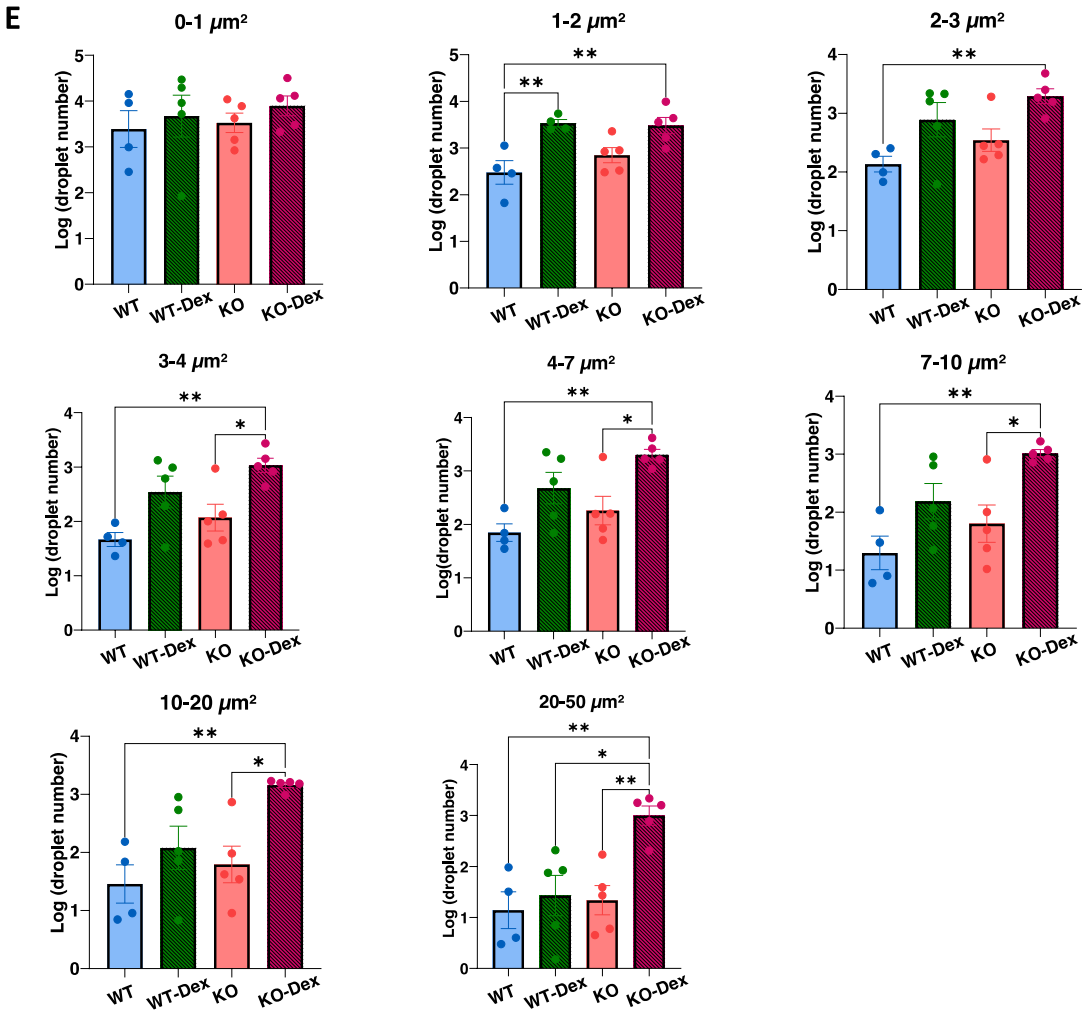
E
0-1 μm²
1-2 μm²
2-3 μm²
3-4 μm²
4-7 μm²
7-10 μm²
10-20 μm²
20-50 μm²
Log (droplet number)
Log(droplet number)
WT
WT-Dex
KO
KO-Dex
**
*

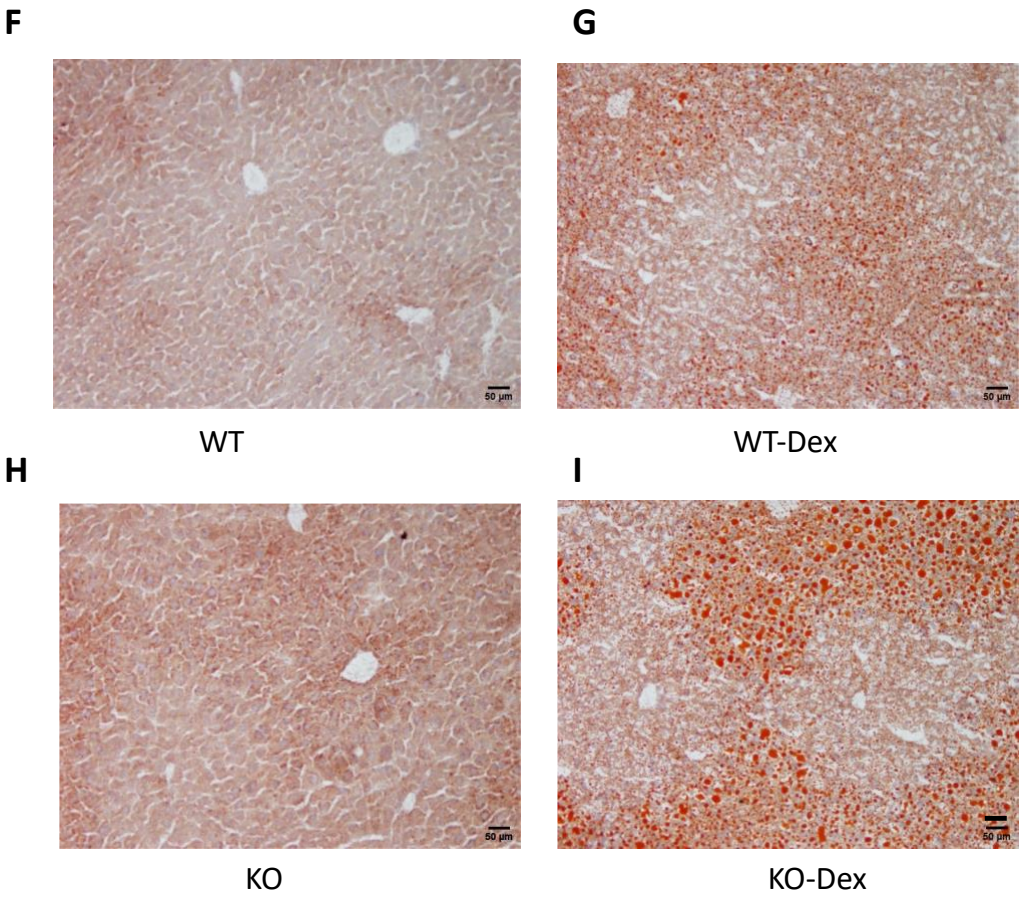

Figure 7: Figure 7: Effect of Dex treatment on liver lipid content in WT and MuRF1-KO mice. WT and MuRF1-KO mice were treated or not with Dex (daily dose of 5 mg/kg in drinking water) for 5 days. A-D, liver slides were used for investigating membrane-linked neutral lipids. The latter were stained using Nile-red (see methods section for details). White bar, 20 µm. Image acquisitions were captured with a high-resolution ORCA-Flash4.0 LT+ Digital CMOS camera coupled to a IX-73 microscope (Olympus). E, membrane-linked lipids from images A-D were quantified using ImageJ (ImageJ2 v. 2.14.0/1.54f) and the data were log10 transformed. Values were grouped by categories of size and analyzed using one-way ANOVA, which showed a global increase of big vesicles in KO animals when compared to WT. Means ± SEM are indicated; significantly different between WT and KO animals, *$p < 0.05$; **, $p < 0.005$. F-I, using companion slides, intracellular neutral lipid droplets were stained using oil red O [25]. Image acquisitions were captured with a DP23 CMOS camera coupled to a IX-73 microscope (Olympus). White bar, 20 µm. Upon Dex-treatment, lipids droplets accumulated but much bigger droplets were observed in KO mice (I) when compared to WT animals (G).

Although modest, significant differences were observed between the liver of WT and MuRF1-KO mice in absence of Dex treatment, as shown by VIP scores extracted from PLS

models (Supplemental Figure 1A): 13 biomarkers were significantly different. This strongly suggests that even in absence of a challenge the deletion of the muscle-specific MuRF1 is not completely neutral for other organs. These data also underscore the usefulness of FTIR investigations that are able to detect variations while no phenotype difference is observed.

Regarding the impact of MuRF1 deletion, we first observed that the liver and the intestine were the most affected organs: liver weight increased markedly in response to Dex. By contrast, intestine weight was depressed upon Dex treatment in WT animals but MuRF1-KO induced a marked increase of intestine weight with or without Dex treatment. The reason of this increase, in particular in non-treated animals, is not clear but this may reflect the long-term adaptation of the organism to the absence of MuRF1 in KO mice. We hypothesize that long-term MuRF1 deletion reduces/alters the exchanges between muscles and the splanchnic area. The liver and intestine hypertrophy in MuRF1-KO mice treated (or not) with Dex may be an overcompensation mechanism allowing the liver and the intestine to increase their energy stores. However, such an adaptation of the organism may be deleterious. Indeed, it is known that high doses of Dex can induce liver steatosis [41], which may be further enhanced if using MuRF1 inhibitors. This suggests that future drugs inhibiting MuRF1 in human for preserving muscle mass during catabolic situations (*e.g.* during idiopathic inflammatory myopathies treated with glucocorticoids [42]) should be optimized both in terms of dose and length of the treatment and that potential side effects have to be investigated in other organs like the liver.

It may be argued that a life-long deletion of MuRF1 may not reflect even a long-term effect of a drug as compensatory mechanisms might have occurred. However, such effects on splanchnic organs (liver and intestine) probably involves a coordinated response of many factors, and an adaptation of the organism seems a logical response to the fact that the splanchnic area cannot rely anymore on muscle to buffer its amino acids and energy needs.

The response of the liver to Dex treatment was similar in wild-type mice and in MuRF1 KO mice, but some effects were exacerbated in MuRF1-KO mice. In particular, the accumulation of lipids in the liver of Dex-treated MuRF1-KO mice was higher than in WT-Dex mice (Figs 5, 7, S1). Similarly, FTIR approach showed that the intensity of the peaks associated with saturated lipids and phospholipids (1465 cm^{-1}) and with triglycerides and phospholipids

(1745 cm^{-1}) were significantly higher in MuRF1-KO mice than in wild-type mice, and increased more in response to Dex treatment.

Short-term Dex treatment reduces fat mass in mice by stimulating fat breakdown in white adipose tissues and increasing brown adipose tissue metabolic activity [34, 43]. This lipolysis releases fatty acids that are oxidized in other tissues like muscles. This oxidation releases glycerol that is used for gluconeogenesis and lipogenesis in liver. Indeed, lipogenesis is stimulated in liver by Dex [44]. Similarly, Dex stimulates the release of amino acids from extra-hepatic tissues that are also used for gluconeogenesis in liver [19, 45]. In MuRF1-KO mice, the effects of Dex on lipolysis in adipose tissue, on gluconeogenesis and lipogenesis in liver should be similar than in WT animals. However, the preservation of muscle in MuRF1-KO animals should concomitantly limit the release of amino acids from muscle, and preserve the capacity of muscle to oxidize fatty acids released from adipose tissue, first because muscle mass is preserved, and second because MuRF1 can inhibit fatty acid oxidation though PPARalpha inhibition [46]. Thus, compared with wild-type animals, the liver of MuRF1-KO mice should receive less amino acids and more glycerol. This could be the mechanism leading to a higher accumulation of lipids in the liver of Dex-treated MuRF1-KO mice. The FTIR also suggested that lipid composition was changed as we observed reduced in 1465 cm^{-1} peaks and increase in 1560 cm^{-1} peaks as a response to the MuRF1 deletion. The peaks associated with saturated lipids (~1465 cm-1) is significantly higher for Dex treatments (KO-Dex and WT-Dex) by comparisons to others (ANOVA, Tukey HSD, $p < 0.01$). As lipid composition greatly influences organelle function and structure [47], more work is clearly needed for investigating the impact of MuRF1-KO on lipid composition and membrane-linked metabolic pathways.

The coupling of FTIR approach and machine learning gave us an objective way to analyze liver cells and identify biomarkers specific to each treatment. Upon MuRF1 deletion, we identified multiple biomarkers supporting the accumulation of glycogen and lipids in liver cells. This accumulation was exacerbated under Dex treatment, which was then confirmed by an enzymatic assay and staining approaches.

Altogether, we found that the deletion of MuRF1 is not as neutral as it was initially suggested [9, 11]. The link between MuRF1 and liver glycogen stores was already described in a model of MuRF1 overexpression in mice [22], but here we describe drastic lipid content modifications in the liver that are exacerbated in Dex-treated animals, and also modest but

significant modifications of protein, carbohydrate and nucleic acids levels. This strengthens our hypothesis that sparing muscle mass must be cautiously investigated.

In conclusion, the lack of MuRF1 in muscles has profound effects in other organs. The composition of proteins, carbohydrates and lipids were markedly altered in Dex-treated mice but FTIR analyses revealed that the deletion of MuRF1 also impacted the liver in non-challenged animals. Future work will have to identify the lipids and proteins modified using omics approaches and to further study the metabolic pathways that may be altered in MuRF1-KO animals. Finally, future drugs aiming at inhibiting MuRF1 will have to take into account their potential side effects in other organs, including, but not limited to, the liver.

Author Contributions: Conceptualization, LM, CP and DT; animal experiments: MD, JD, JH, MM; data acquisition CC-G, MM, AC; data processing: CD, LM; interpretation of data, DT, LM, AG, A-CM; writing—original draft preparation, DT, LM; writing—review and editing LM, DT, AG, A-CM, CP, LC, PF; funding acquisition, PF, A-CM, DT. All authors have read and agreed to the published version of the manuscript.

Funding: This work was supported by grants from the AFM-Telethon (grant #19521) and from the Fondation pour la Recherche Médicale (labelling FRM, labelling FRM, DEQ20180339180).

Acknowledgements: The authors would like to thank Pr. S. Labeit (Medical Faculty Mannheim, University of Heidelberg) and Pr. V. Adams (Heart Center Dresden) for their generous gift of MuRF1-KO mice.
The authors are supported by the French "Institut National de Recherche pour l'Agriculture, l'alimentation et l'Environnement" (INRAE).

Supporting information:
Supplementary Figure 1: VIP scores extracted from PLS-DA model testing the MuRF1 mutation effect by comparing WT and KO mice without Dex treatment.

References

(1) Jonker, R.; Engelen, M. P.; Deutz, N. E. Role of specific dietary amino acids in clinical conditions. *Br J Nutr* **2012**, *108 Suppl 2* (0 2), S139-148. DOI: 10.1017/S0007114512002358.
(2) Gabay, C.; Kushner, I. Acute-phase proteins and other systemic responses to inflammation. *N Engl J Med* **1999**, *340* (6), 448-454. DOI: 10.1056/NEJM199902113400607.
(3) Obled, C.; Papet, I.; Breuille, D. Metabolic bases of amino acid requirements in acute diseases. *Curr Opin Clin Nutr Metab Care* **2002**, *5* (2), 189-197. DOI: 10.1097/00075197-200203000-00012. Richardson, R. A.; Davidson, H. I. Nutritional demands in acute and chronic illness. *Proc Nutr Soc* **2003**, *62* (4), 777-781. DOI: 10.1079/PNS2003302.
(4) Rennie, M. J.; Tipton, K. D. Protein and amino acid metabolism during and after exercise and the effects of nutrition. *Annu Rev Nutr* **2000**, *20*, 457-483. DOI: 10.1146/annurev.nutr.20.1.457. Petersen, K. F.; Dufour, S.; Cline, G. W.; Shulman, G. I. Regulation of hepatic mitochondrial oxidation by glucose-alanine cycling during starvation in humans. *J Clin Invest* **2019**, *129* (11), 4671-4675. DOI: 10.1172/JCI129913.
(5) Fearon, K.; Arends, J.; Baracos, V. Understanding the mechanisms and treatment options in cancer cachexia. *Nat Rev Clin Oncol* **2013**, *10* (2), 90-99. DOI: 10.1038/nrclinonc.2012.209. von Haehling, S.; Anker, M. S.; Anker, S. D. Prevalence and clinical impact of cachexia in chronic illness in

Europe, USA, and Japan: facts and numbers update 2016. *J Cachexia Sarcopenia Muscle* **2016**, *7* (5), 507-509. DOI: 10.1002/jcsm.12167.
(6) Sandri, M. Protein breakdown in muscle wasting: role of autophagy-lysosome and ubiquitin-proteasome. *Int J Biochem Cell Biol* **2013**, *45* (10), 2121-2129. DOI: 10.1016/j.biocel.2013.04.023.
(7) Wang, Y.; Pessin, J. E. Mechanisms for fiber-type specificity of skeletal muscle atrophy. *Curr Opin Clin Nutr Metab Care* **2013**, *16* (3), 243-250. DOI: 10.1097/MCO.0b013e328360272d. Talbot, J.; Maves, L. Skeletal muscle fiber type: using insights from muscle developmental biology to dissect targets for susceptibility and resistance to muscle disease. *Wiley Interdiscip Rev Dev Biol* **2016**, *5* (4), 518-534. DOI: 10.1002/wdev.230.
(8) Milan, G.; Romanello, V.; Pescatore, F.; Armani, A.; Paik, J. H.; Frasson, L.; Seydel, A.; Zhao, J.; Abraham, R.; Goldberg, A. L.; et al. Regulation of autophagy and the ubiquitin-proteasome system by the FoxO transcriptional network during muscle atrophy. *Nat Commun* **2015**, *6*, 6670. DOI: 10.1038/ncomms7670. Kotter, S.; Kruger, M. Protein Quality Control at the Sarcomere: Titin Protection and Turnover and Implications for Disease Development. *Front Physiol* **2022**, *13*, 914296. DOI: 10.3389/fphys.2022.914296.
(9) Bodine, S. C.; Latres, E.; Baumhueter, S.; Lai, V. K.; Nunez, L.; Clarke, B. A.; Poueymirou, W. T.; Panaro, F. J.; Na, E.; Dharmarajan, K.; et al. Identification of ubiquitin ligases required for skeletal muscle atrophy. *Science* **2001**, *294* (5547), 1704-1708. DOI: 10.1126/science.1065874.
(10) Polge, C.; Cabantous, S.; Deval, C.; Claustre, A.; Hauvette, A.; Bouchenot, C.; Aniort, J.; Bechet, D.; Combaret, L.; Attaix, D.; et al. A muscle-specific MuRF1-E2 network requires stabilization of MuRF1-E2 complexes by telethonin, a newly identified substrate. *J Cachexia Sarcopenia Muscle* **2018**, *9* (1), 129-145. DOI: 10.1002/jcsm.12249. Kedar, V.; McDonough, H.; Arya, R.; Li, H. H.; Rockman, H. A.; Patterson, C. Muscle-specific RING finger 1 is a bona fide ubiquitin ligase that degrades cardiac troponin I. *Proc Natl Acad Sci U S A* **2004**, *101* (52), 18135-18140. DOI: 10.1073/pnas.0404341102.
(11) Peris-Moreno, D.; Taillandier, D.; Polge, C. MuRF1/TRIM63, Master Regulator of Muscle Mass. *Int J Mol Sci* **2020**, *21* (18). DOI: 10.3390/ijms21186663.
(12) Polge, C.; Aniort, J.; Armani, A.; Claustre, A.; Coudy-Gandilhon, C.; Tournebize, C.; Deval, C.; Combaret, L.; Béchet, D.; Sandri, M.; et al. UBE2E1 Is Preferentially Expressed in the Cytoplasm of Slow-Twitch Fibers and Protects Skeletal Muscles from Exacerbated Atrophy upon Dexamethasone Treatment. *Cells* **2018**, *7* (11). DOI: 10.3390/cells7110214.
(13) Neyroud, D.; Laitano, O.; Dasgupta, A.; Lopez, C.; Schmitt, R. E.; Schneider, J. Z.; Hammers, D. W.; Sweeney, H. L.; Walter, G. A.; Doles, J.; et al. Blocking muscle wasting via deletion of the muscle-specific E3 ligase MuRF1 impedes pancreatic tumor growth. *Commun Biol* **2023**, *6* (1), 519. DOI: 10.1038/s42003-023-04902-2.
(14) Adams, V.; Bowen, T. S.; Werner, S.; Barthel, P.; Amberger, C.; Konzer, A.; Graumann, J.; Sehr, P.; Lewis, J.; Provaznik, J.; et al. Small-molecule-mediated chemical knock-down of MuRF1/MuRF2 and attenuation of diaphragm dysfunction in chronic heart failure. *J Cachexia Sarcopenia Muscle* **2019**, *10* (5), 1102-1115. DOI: 10.1002/jcsm.12448. Bowen, T. S.; Adams, V.; Werner, S.; Fischer, T.; Vinke, P.; Brogger, M. N.; Mangner, N.; Linke, A.; Sehr, P.; Lewis, J.; et al. Small-molecule inhibition of MuRF1 attenuates skeletal muscle atrophy and dysfunction in cardiac cachexia. *J Cachexia Sarcopenia Muscle* **2017**, *8* (6), 939-953. DOI: 10.1002/jcsm.12233.
(15) Ribeiro, F.; Alves, P. K. N.; Bechara, L. R. G.; Ferreira, J. C. B.; Labeit, S.; Moriscot, A. S. Small-Molecule Inhibition of MuRF1 Prevents Early Disuse-Induced Diaphragmatic Dysfunction and Atrophy. *Int J Mol Sci* **2023**, *24* (4). DOI: 10.3390/ijms24043637.
(16) Smith, J. G.; Koronowski, K. B.; Mortimer, T.; Sato, T.; Greco, C. M.; Petrus, P.; Verlande, A.; Chen, S.; Samad, M.; Deyneka, E.; et al. Liver and muscle circadian clocks cooperate to support glucose tolerance in mice. *Cell Rep* **2023**, *42* (6), 112588. DOI: 10.1016/j.celrep.2023.112588.
(17) Ma, R.; Zhang, W.; Tang, K.; Zhang, H.; Zhang, Y.; Li, D.; Li, Y.; Xu, P.; Luo, S.; Cai, W.; et al. Switch of glycolysis to gluconeogenesis by dexamethasone for treatment of hepatocarcinoma. *Nat Commun* **2013**, *4*, 2508. DOI: 10.1038/ncomms3508. Goldberg, D.; Charni-Natan, M.; Buchshtab, N.; Bar-Shimon, M.; Goldstein, I. Hormone-controlled cooperative binding of transcription factors drives

synergistic induction of fasting-regulated genes. *Nucleic Acids Res* **2022**, *50* (10), 5528-5544. DOI: 10.1093/nar/gkac358.
(18) Sistare, F. D.; Haynes, R. C., Jr. Acute stimulation by glucocorticoids of gluconeogenesis from lactate/pyruvate in isolated hepatocytes from normal and adrenalectomized rats. *J Biol Chem* **1985**, *260* (23), 12754-12760.
(19) Kuo, T.; Harris, C. A.; Wang, J. C. Metabolic functions of glucocorticoid receptor in skeletal muscle. *Mol Cell Endocrinol* **2013**, *380* (1-2), 79-88. DOI: 10.1016/j.mce.2013.03.003.
(20) Savary, I.; Debras, E.; Dardevet, D.; Rambourdin, F.; Vasson, M. P.; Obled, C.; Grizard, J. Evidence for an alteration of plasma and liver proteins response to dexamethasone in aging rats. *Mech Ageing Dev* **2001**, *122* (1), 105-120. DOI: 10.1016/s0047-6374(00)00224-4.
(21) Wang, C. N.; McLeod, R. S.; Yao, Z.; Brindley, D. N. Effects of dexamethasone on the synthesis, degradation, and secretion of apolipoprotein B in cultured rat hepatocytes. *Arterioscler Thromb Vasc Biol* **1995**, *15* (9), 1481-1491. DOI: 10.1161/01.atv.15.9.1481.
(22) Hirner, S.; Krohne, C.; Schuster, A.; Hoffmann, S.; Witt, S.; Erber, R.; Sticht, C.; Gasch, A.; Labeit, S.; Labeit, D. MuRF1-dependent regulation of systemic carbohydrate metabolism as revealed from transgenic mouse studies. *J Mol Biol* **2008**, *379* (4), 666-677. DOI: 10.1016/j.jmb.2008.03.049.
(23) Liu, S.; Brown, J. D.; Stanya, K. J.; Homan, E.; Leidl, M.; Inouye, K.; Bhargava, P.; Gangl, M. R.; Dai, L.; Hatano, B.; et al. A diurnal serum lipid integrates hepatic lipogenesis and peripheral fatty acid use. *Nature* **2013**, *502* (7472), 550-554. DOI: 10.1038/nature12710.
(24) D. Keppler, K. D. *Glycogen determination with amylo-glucosidase*; 1974.
(25) Mehlem, A.; Hagberg, C. E.; Muhl, L.; Eriksson, U.; Falkevall, A. Imaging of neutral lipids by oil red O for analyzing the metabolic status in health and disease. *Nat Protoc* **2013**, *8* (6), 1149-1154. DOI: 10.1038/nprot.2013.055.
(26) Lieber, C. A.; Mahadevan-Jansen, A. Automated method for subtraction of fluorescence from biological Raman spectra. *Appl Spectrosc* **2003**, *57* (11), 1363-1367. DOI: 10.1366/000370203322554518.
(27) Demšar, J.; Curk, T.; Erjavec, A.; Gorup, Č.; Hočevar, T.; Milutinovič, M.; Možina, M.; Polajnar, M.; Toplak, M.; Starič, A.; et al. Orange: Data Mining Toolbox in Python. *Journal of Machine Learning Research* **2013**, 2349-2353.
(28) Ferrer, M.; Mourikis, N.; Davidson, E. E.; Kleeman, S. O.; Zaccaria, M.; Habel, J.; Rubino, R.; Gao, Q.; Flint, T. R.; Young, L.; et al. Ketogenic diet promotes tumor ferroptosis but induces relative corticosterone deficiency that accelerates cachexia. *Cell Metab* **2023**, *35* (7), 1147-1162 e1147. DOI: 10.1016/j.cmet.2023.05.008. Chen, H. L.; Romsos, D. R. A single intracerebroventricular injection of dexamethasone elevates food intake and plasma insulin and depresses metabolic rates in adrenalectomized obese (ob/ob) mice. *J Nutr* **1995**, *125* (3), 540-545. DOI: 10.1093/jn/125.3.540.
(29) Jahng, J. W.; Kim, N. Y.; Ryu, V.; Yoo, S. B.; Kim, B. T.; Kang, D. W.; Lee, J. H. Dexamethasone reduces food intake, weight gain and the hypothalamic 5-HT concentration and increases plasma leptin in rats. *Eur J Pharmacol* **2008**, *581* (1-2), 64-70. DOI: 10.1016/j.ejphar.2007.11.029.
(30) Polge, C.; Aniort, J.; Armani, A.; Claustre, A.; Coudy-Gandilhon, C.; Tournebize, C.; Deval, C.; Combaret, L.; Bechet, D.; Sandri, M.; et al. Erratum: Polge, C., et al. UBE2E1 Is Preferentially Expressed in the Cytoplasm of Slow-Twitch Fibers and Protects Skeletal Muscles from Exacerbated Atrophy upon Dexamethasone Treatment. Cells 2018, 7, 214. *Cells* **2018**, *7* (12). DOI: 10.3390/cells7120242.
(31) Lindqvist, J.; Kolb, J.; de Winter, J.; Tonino, P.; Hourani, Z.; Labeit, S.; Ottenheijm, C.; Granzier, H. Removal of MuRF1 Increases Muscle Mass in Nemaline Myopathy Models, but Does Not Provide Functional Benefits. *Int J Mol Sci* **2022**, *23* (15). DOI: 10.3390/ijms23158113.
(32) Willis, M. S.; Ike, C.; Li, L.; Wang, D. Z.; Glass, D. J.; Patterson, C. Muscle ring finger 1, but not muscle ring finger 2, regulates cardiac hypertrophy in vivo. *Circ Res* **2007**, *100* (4), 456-459. DOI: 10.1161/01.RES.0000259559.48597.32. Maejima, Y.; Usui, S.; Zhai, P.; Takamura, M.; Kaneko, S.; Zablocki, D.; Yokota, M.; Isobe, M.; Sadoshima, J. Muscle-specific RING finger 1 negatively regulates pathological cardiac hypertrophy through downregulation of calcineurin A. *Circ Heart Fail* **2014**, *7* (3), 479-490. DOI: 10.1161/CIRCHEARTFAILURE.113.000713.

(33) Smyth, T.; Totemeyer, S.; Haugland, S.; Willers, C.; Peters, S.; Maskell, D.; Bryant, C. Dexamethasone modulates Salmonella enterica serovar Typhimurium infection in vivo independently of the glucocorticoid-inducible protein annexin-A1. *FEMS Immunol Med Microbiol* **2008**, *54* (3), 339-348. DOI: 10.1111/j.1574-695X.2008.00485.x.
(34) Koorneef, L. L.; van der Meulen, M.; Kooijman, S.; Sanchez-Lopez, E.; Scheerstra, J. F.; Voorhoeve, M. C.; Ramesh, A. N. N.; Rensen, P. C. N.; Giera, M.; Kroon, J.; et al. Dexamethasone-associated metabolic effects in male mice are partially caused by depletion of endogenous corticosterone. *Front Endocrinol (Lausanne)* **2022**, *13*, 960279. DOI: 10.3389/fendo.2022.960279.
(35) Zohdi, V.; Whelan, D. R.; Wood, B. R.; Pearson, J. T.; Bambery, K. R.; Black, M. J. Importance of tissue preparation methods in FTIR micro-spectroscopical analysis of biological tissues: 'traps for new users'. *PLoS One* **2015**, *10* (2), e0116491. DOI: 10.1371/journal.pone.0116491.
(36) Ji, Y.; Yang, X.; Ji, Z.; Zhu, L.; Ma, N.; Chen, D.; Jia, X.; Tang, J.; Cao, Y. DFT-Calculated IR Spectrum Amide I, II, and III Band Contributions of N-Methylacetamide Fine Components. *ACS Omega* **2020**, *5* (15), 8572-8578. DOI: 10.1021/acsomega.9b04421.
(37) Allan, C.; Burel, J-M.; Moore, J.; Blackburn, C.; Linkert, M.; Loynton, S.; MacDonald, D.; Moore, W. J.; Neves, C.; Patterson, A.; et al. OMERO: flexible, model-driven data management for experimental biology. *Nat Methods* **2012,** *9*, 245–253. DOI:10.1038/nmeth.1896
(38) Zhanghao, K.; Liu, W.; Li, M.; Wu, Z.; Wang, X.; Chen, X.; Shan, C.; Wang, H.; Chen, X.; Dai, Q.; et al. High-dimensional super-resolution imaging reveals heterogeneity and dynamics of subcellular lipid membranes. *Nat Commun* **2020**, *11* (1), 5890. DOI: 10.1038/s41467-020-19747-0.
(39) O'Rourke, E. J.; Soukas, A. A.; Carr, C. E.; Ruvkun, G. C. elegans major fats are stored in vesicles distinct from lysosome-related organelles. *Cell Metab* **2009**, *10* (5), 430-435. DOI: 10.1016/j.cmet.2009.10.002.
(40) Jiao, T.; Yao, X.; Zhao, Y.; Zhou, Y.; Gao, Y.; Fan, S.; Chen, P.; Li, X.; Jiang, Y.; Yang, X.; et al. Dexamethasone-Induced Liver Enlargement Is Related to PXR/YAP Activation and Lipid Accumulation but Not Hepatocyte Proliferation. *Drug Metab Dispos* **2020**, *48* (9), 830-839. DOI: 10.1124/dmd.120.000061. Harno, E.; Sefton, C.; Wray, J. R.; Allen, T. J.; Davies, A.; Coll, A. P.; White, A. Chronic glucocorticoid treatment induces hepatic lipid accumulation and hyperinsulinaemia in part through actions on AgRP neurons. *Sci Rep* **2021**, *11* (1), 13776. DOI: 10.1038/s41598-021-93378-3.
(41) Du, W. W.; Liu, F.; Shan, S. W.; Ma, X. C.; Gupta, S.; Jin, T.; Spaner, D.; Krylov, S. N.; Zhang, Y.; Ling, W.; et al. Inhibition of Dexamethasone-induced Fatty Liver Development by Reducing miR-17-5p Levels. *Mol Ther* **2015**, *23* (7), 1222-1233. DOI: 10.1038/mt.2015.64.
(42) Hanaoka, B. Y.; Peterson, C. A.; Horbinski, C.; Crofford, L. J. Implications of glucocorticoid therapy in idiopathic inflammatory myopathies. *Nat Rev Rheumatol* **2012**, *8* (8), 448-457. DOI: 10.1038/nrrheum.2012.85.
(43) Peckett, A. J.; Wright, D. C.; Riddell, M. C. The effects of glucocorticoids on adipose tissue lipid metabolism. *Metabolism* **2011**, *60* (11), 1500-1510. DOI: 10.1016/j.metabol.2011.06.012.
(44) Wang, Z.; Iwasaki, Y.; Zhao, L. F.; Nishiyama, M.; Taguchi, T.; Tsugita, M.; Kambayashi, M.; Hashimoto, K.; Terada, Y. Hormonal regulation of glycolytic enzyme gene and pyruvate dehydrogenase kinase/phosphatase gene transcription. *Endocr J* **2009**, *56* (8), 1019-1030. DOI: 10.1507/endocrj.k09e-178.
(45) Kim, Y.; Park, S.; Lee, J.; Jang, J.; Jung, J.; Koh, J. H.; Choi, C. S.; Wolfe, R. R.; Kim, I. Y. Essential Amino Acid-Enriched Diet Alleviates Dexamethasone-Induced Loss of Muscle Mass and Function through Stimulation of Myofibrillar Protein Synthesis and Improves Glucose Metabolism in Mice. *Metabolites* **2022**, *12* (1). DOI: 10.3390/metabo12010084.
(46) Rodriguez, J. E.; Liao, J. Y.; He, J.; Schisler, J. C.; Newgard, C. B.; Drujan, D.; Glass, D. J.; Frederick, C. B.; Yoder, B. C.; Lalush, D. S.; et al. The ubiquitin ligase MuRF1 regulates PPARalpha activity in the heart by enhancing nuclear export via monoubiquitination. *Mol Cell Endocrinol* **2015**, *413*, 36-48. DOI: 10.1016/j.mce.2015.06.008. Quintana, M. T.; He, J.; Sullivan, J.; Grevengoed, T.; Schisler, J.; Han, Y.; Hill, J. A.; Yates, C. C.; Stansfield, W. E.; Mapanga, R. F.; et al. Muscle ring finger-3 protects against diabetic cardiomyopathy induced by a high fat diet. *BMC Endocr Disord* **2015**, *15*, 36. DOI: 10.1186/s12902-015-0028-z.

(47) Renard, K.; Byrne, B. Insights into the Role of Membrane Lipids in the Structure, Function and Regulation of Integral Membrane Proteins. *Int J Mol Sci* **2021**, *22* (16). DOI: 10.3390/ijms22169026.
Casares, D.; Escriba, P. V.; Rossello, C. A. Membrane Lipid Composition: Effect on Membrane and Organelle Structure, Function and Compartmentalization and Therapeutic Avenues. *Int J Mol Sci* **2019**, *20* (9). DOI: 10.3390/ijms20092167.

for Table of Contents use only

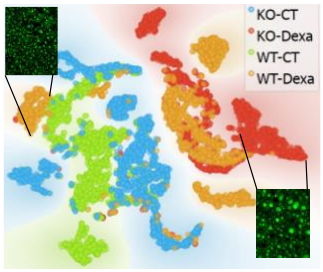

Liver lipid accumulation is a major side effect in muscle-specific MuRF1-KO mice